Ab Initio Optical Absorption Spectra of Size-Expanded xDNA Base Assemblies

ARTICLE *in* THE JOURNAL OF PHYSICAL CHEMISTRY B · JANUARY 2008

Impact Factor: 3.3 · DOI: 10.1021/jp075711z · Source: PubMed

3 AUTHORS, INCLUDING:

Daniele Varsano
Italian National Research Council
39 PUBLICATIONS **999** CITATIONS
SEE PROFILE

Rosa Di Felice
Italian National Research Council
143 PUBLICATIONS **3,018** CITATIONS
SEE PROFILE

Ab Initio Optical Absorption Spectra of Size-Expanded xDNA Base Assemblies

Daniele Varsano,* Anna Garbesi, and Rosa Di Felice*

National Center on nanoStructures and bioSystems at Surfaces (S3) of INFM-CNR, c/o Dipartimento di Fisica, Universita di Modena e Reggio Emilia, Via Campi 213/A, 41100 Modena, Italy

Received: July 20, 2007; In Final Form: August 29, 2007

We present the results of time-dependent density functional theory calculations of the optical absorption spectra of synthetic nucleobases and of their hydrogen-bonded and stacked base pairs. We focus on size-expanded analogues of the natural nucleobases obtained through the insertion of a benzene ring bonded to the planar heterocycles (x-bases), according to the protocol designed and realized by the group of Eric Kool (e.g., see: Gao, J.; Liu, H.; Kool, E.T. *Angew. Chem., Int. Ed.* **2005**, *44*, 3118, and references therein). We find that the modifications of the frontier electron orbitals with respect to natural bases, which are induced by the presence of the aromatic ring, also affect the optical response. In particular, the absorption onset is pinned by the benzene component of the HOMO of each x-base (xA, xG, xT, xC). In addition, the main trait of the H-bonding interbase coupling is a conspicuous red shift of spectral peaks in the low-energy range. Finally, the hypochromicity, a well-known fingerprint of stacking, is more pronounced in stacked xG−C and xA−T pairs than that in stacked G−C and A−T pairs, an index of enhanced stacking.

I. Introduction

A long-standing target of scientists in different disciplines is the pursuit of a genetic system with a greater capacity of storing and transmitting information than that of natural DNA. Such a goal would have enormous biological implications[1] and, at the same time, could have impact in the design and realization of biotechnology concepts.[2] The routes of biomimetic chemistry and synthetic biology are followed,[3,4] with the strategy of searching alternative nucleobases that, on one hand, may be put in a sequence and implement self-assembly with a high recognition and selectivity yield and, on the other hand, may undergo self-templated growth and replication by suitable enzymes (e.g., polymerases). Within this effort, several research laboratories are active worldwide in the design of nucleobase mimics that can form DNA-like double helices along with the natural bases. Several different synthesis protocols are implemented, ranging from modifying the base heterocycles to changing the backbone, as summarized in recent reviews.[1,5−7] We focus here on systems obtained by one particular approach, implemented by Kool's laboratory. This approach relies on the expansion of each natural base with a benzene ring that is covalently bonded to the base and coplanar with it (see Figure 1).

Kool's group followed a precise path during the last 4 years, composed of consequential steps. The first step was the optimization of the synthesis procedure of single modified bases with the insertion of aromatic rings.[8−11] Then, they demonstrated that such base analogues are able to pair with natural DNA bases by H bonding, forming base pairs of expanded size.[9,12] Finally, they showed that such expanded base pairs stack with each other and with natural base pairs, assembling helical motifs.[8,10,13−15] Double helices of this kind are more stable than natural Watson−Crick DNA if solely expanded base pairs occur, whereas they are less stable than natural DNA if both expanded and natural base pairs compose the sequence.[8] From the combined analysis of thermal denaturation data and NMR structural data, this interesting outcome was interpreted as a consequence of enhanced stacking either within each strand or across the strands.[8] This latter characteristic, which is also revealed in the reduced average stacking distance of 3.1 Å in some xDNA double helices[13] (instead of 3.4 Å), are turning the attention of researchers for such systems to nanoelectronic applications. In fact, enhanced stacking may translate into an enhanced $\pi-\pi$ overlap through the stack and therefore into more delocalized electron orbitals and better conductivity. Indeed, the fact that reducing the stacking distance results into larger bandwidths and smaller band gaps was recently proven in the context of G4-DNA.[16] The higher stability of xDNA relative to natural DNA may be exploited not only for nanoelectronics applications but also for bionanotechnology at large because stiffer structures are potentially more resistant to the strong forces exerted by the inorganic materials such as substrates, electrodes, and functional nanoparticles to which they are normally coupled for measuring and functioning.

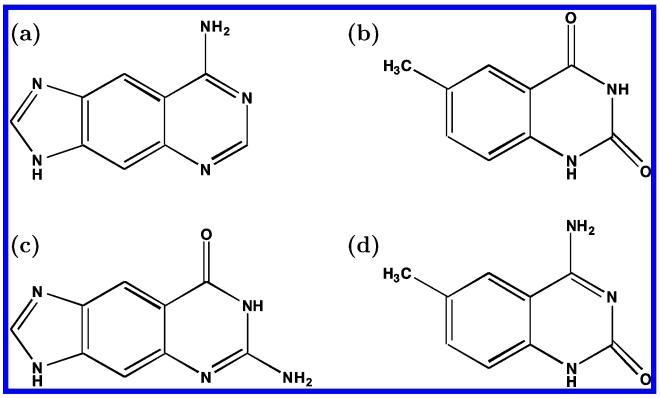

Figure 1. Structures of the size-expanded x-bases (a) xA, (b) xT, (c) xG, and (d) xC.

* To whom correspondence should be addressed. E-mail: varsano.daniele@unimore.it (D.V.); rosa@unimore.it (R.D.F.).

10.1021/jp075711z CCC: $37.00
Published on Web 11/23/2007

To test this intriguing hypothesis for xDNA, Hartree−Fock and density functional theory (DFT) studies of the electronic structure of x-bases and x-base pairs have lately been performed [17−22]. Fuentes-Cabrera and co-workers carried out a series of calculations on isolated x-bases aimed at investigating (i) whether the highest occupied molecular orbital (HOMO) and the lowest unoccupied molecular orbital (LUMO) contain charge contribution from the fused benzene ring;[17,18] (ii) whether the aromatic expansion induces changes in the electron energy levels in a way that is promising for nanowire applications;[2,17,18] (iii) whether nonplanarity is important in these molecules;[17,18] and (iv) to which extent the HOMO−LUMO gap can be controlled by varying the degree of aromaticity in different tautomers.[19,20] More recently, they turned their attention to an xDNA realistic stack.[22] Stacking effects were also thoroughly analyzed by McConnell and Wetmore.[21] Concisely, all of these computational studies confirmed Kool's suggestion of enhanced stacking interactions due to the presence of the additional aromatic charge in the frontier orbitals.

In the stream of such ground-state electronic structure calculations, we now turn our attention to the excited-state properties of x-bases and few representative x-base assemblies, namely, H-bonded xG−C and xA−T pairs and stacks of H-bonded xG−C and xA−T pairs. We compute the optical absorption spectra by time-dependent density functional theory (TDDFT) in the real-space real-time implementation. Our aim is to understand which marks are imprinted in the optical spectra by the additional aromatic charge revealed from the ground-state calculations in the HOMO and LUMO and in other electron orbitals.[17] Optical characterization techniques are standard postsynthesis methods adopted in any chemistry laboratory and were used to identify the peculiar traits of xDNA with respect to natural DNA.[9,11] Therefore, it is extremely valuable to have an ab initio theoretical counterpart to interpret the data and possibly generalize the physicochemical effects, and we start from the building blocks. Furthermore, knowledge of the optical response is, in principle, connected to issues such as conductivity[23,24a] and UV irradiation and damage,[24,25] as was pursued for natural DNA [23−25]. We find that the optical absorption spectra of isolated x-bases are in fair qualitative agreement with experimental data, to a degree of accuracy that is expected for this level of theory. All of the x-bases are characterized by an absorption onset peak at lower energy than that in natural DNA, as expected on the basis of the reduced HOMO−LUMO gap. Most interestingly, we discuss how the well-known effects of red shift and hypochromicity upon H bonding and stacking manifest in these systems, particularly focusing on the similarities and differences with respect to natural DNA.

The paper is organized as follows. In section II, we shortly describe the real-time real-space TDDFT method adopted to compute the optical properties. In section III, we present our results for the isolated gas-phase xDNA bases, indicated with xG, xC, xA, and xT. To understand the role of hydrogen bonding in shifts and modifications of the spectral features, we report and discuss, in section IV, results for H-bonded Watson−Crick xG−C and xA−T pairs. In section V, we present results of the optical absorption of systems made of two stacked H-bonded Watson−Crick x-pairs. In sections III, IV, and VCITE, for each system, we briefly comment on the salient traits of the ground-state electronic properties and then move to the optical excitations. In section VI, we summarize the results of the present work.

II. Computational Framework

Our procedure relies on density functional theory and is briefly explained in the following. For the geometries listed above and explained in more detail in the next sections, we obtained the optical spectra within time-dependent density functional theory[26,27] using a real-space, real-time approach to solve the time-dependent Kohn−Sham equations, as implemented in the computer code OCTOPUS.[28,29] Calculations were performed at zero temperature and fixed geometries. The electron−ion interaction was described through norm-conserving pseudopotentials.[30] The LDA parametrization[31] (adiabatic approximation) for the exchange and correlation potential was employed during the time evolution.

In a typical calculation, for example, for each chosen structure, as a first step, the ground state of the system is computed in the DFT framework; we use both LDA and gradient-corrected (GGA) exchange−correlation functionals for the isolated bases and only the LDA functional for the x-pairs and x-pair dimers. Then, to calculate the optical response, the system is excited from its ground state by applying an instantaneous (delta-like) electric field $E_0\delta(t)$. From the Fourier transform of the real-time response to this perturbation, the dynamical polarizability $\alpha(E)$ is obtained in the frequency range of interest. The dipole strength function $S(E)$, which is proportional to the absorption cross section, is finally obtained from the relation

$$S(E) = \frac{2mE}{\hbar^2 e^2 \pi} \mathscr{T} \frac{1}{3} \sum_{\nu} \alpha_{\nu}(E) \qquad (1)$$

where ν stands for each of the three principal Cartesian directions along which the system is perturbed by the delta-like electric field. Within such a scheme, we adopt the following technical parameters. To represent the wave functions in the real space, we use a uniform grid made of overlapping spheres with a radius of 5 Å centered around each nucleus, with a grid spacing of 0.23 Å. For the integration of the time-dependent Kohn−Sham equations, we use the Lanczos algorithm.[41] A time step of 0.007 fs assures the stability of the time propagation. A total propagation time of 20 fs results in a resolution of about 0.1 eV in the computed spectrum.[33] The accuracy in reproducing transitions of intermediate energy is known to be somewhat deteriorated due to the wrong asymptotic behavior of the LDA exchange−correlation potential. For this reason, we will focus the analysis of our results on the peaks in a finite low-energy range of ∼3−6 eV (∼200−400 nm).

A significant advantage of this real-time approach is the fact that only occupied states are needed, thus avoiding the cumbersome calculation of the unoccupied states that instead enter the traditional orbital representation of the linear response equation.[32] The complete set of empty orbitals required in the latter approach is fully accounted for by the time propagation in our approach. In addition, it is important to note that in the time domain, only the approximation to the exchange−correlation potential V_{xc} is required, whereas in conventional frequency−domain linear response TDDFT formulations, the f_{xc} kernel is needed. For a more detailed description of the applied method, we refer the reader to the original publications.[28,33] This approach has already been used for the study of metal and semiconducting clusters,[33,34] aromatic molecules,[35,36] protein chromophores,[37,38] and natural DNA bases and base assemblies.[39] Moreover, it proved quite successful in distinguishing the different isomers of C_{20}.[40] When experimental spectra were available for a direct comparison, TDDFT within an adiabatic

TABLE 1: Kohn−Sham HOMO−LUMO Gap at the LDA (GGA/PBE) Level, for Size-Expanded xDNA and Natural DNA Bases, Compared with Other DFT Computational Results

	Kohn−Sham HOMO−LUMO energy gap (eV)			
	this DFT work		previous DFT work	
base	xDNA	DNA	xDNA[a]	DNA[b]
adenine	2.83 (2.84)	3.80	2.90	3.84
cytosine	2.93 (2.95)	3.57	3.04	3.64
guanine	3.05 (3.06)	3.88	3.16	3.85
thymine	3.30 (3.33)	3.66	3.40	3.76

[a] Computed at the LDA level with localized basis functions, from ref 17. [b] Computed at the GGA/PW91 level with plane wave basis sets, from ref 17.

local density (LDA) or an adiabatic generalized gradient approximation (GGA) to the exchange−correlation function reproduced the low-energy peaks of the optical spectra with a typical accuracy of 0.1 eV.[33] This fair accuracy is not obtained, on the contrary, if one takes the differences of the eigenvalues of the HOMO and the LUMO; the latter procedure, in fact, yields peaks at lower frequencies, in disagreement with the experimental spectra for the well-known underestimate of the DFT fundamental energy gap.

III. Isolated x-Bases

As described in the previous section, the first step of our work is the knowledge of the ground-state Kohn−Sham wave functions. The ground-state electronic properties for the four x-bases have been computed at LDA and GGA/PBE[42] levels. The DFT ground state has been achieved in a real-space grid with the same parameters for the box shape, volume, and grid spacing that have subsequently been used for the time evolution. We assumed the geometries obtained by structural optimization at the MP2/6-31G** level[17] and did not perform any further atomic relaxation.

The calculated HOMO−LUMO energy gaps in electronvolts in the LDA (GGA) approximation are reported in Table 1, together with the values for the natural bases calculated with the same method as that used by us in a previous work[39] and the results on DNA and xDNA bases by other authors.[17] Our results for both natural and benzo-fused bases have the same trend as those from previous DFT calculations[17] and are in good agreement with them, C < T < A < G, xA < xC < xG < xT, with similar energy differences between the various bases. This ensures a comparable degree of convergence with respect to the basis set size, despite the use of different basis sets; in fact, we adopt a uniform grid as described in the previous section, whereas Fuentes-Cabrera and co-workers adopted a localized basis set for the LDA calculations and a plane wave basis set for the GGA calculations. We observe that the use of the gradient-corrected functional does not give substantial changes with respect to the local approximation. In agreement with ref 17, we find that at the DFT level, the HOMO−LUMO energy gap of the x-bases is always lower than that for the natural DNA bases. Although the absolute value of the ground-state HOMO−LUMO gap is always underestimated by the DFT approach, we believe that the systematic decrease in passing from natural to benzo-fused bases is reliable. As already pointed out,[17] this feature may have important consequences on the capability of transporting mobile charges in view of nanoelectronic applications.

It is known that in natural DNA, guanine has the lowest ionization potential (IP). Our calculations indicate that this is true also for the benzo-expanded counterpart; the IP of xG is the lowest ionization potential among the x-bases, and it is similar to the IP of natural guanine, slightly smaller by 0.02 eV. A comparable result was also found in the previous DFT investigation of x-bases; Fuentes-Cabrera and co-workers[17] reported that the HOMO of xG is 0.08 eV higher than the HOMO of G (equivalent to saying that the IP is smaller by this amount). We remark that the IP is another quantity related to the ability of DNA oligomers to sustain charge motion, in connection to the mechanisms of electron/hole transfer through oligomers in solution.[43] If one takes into account the state-of-the-art knowledge about the consequences of the lowest guanine oxidation potential in natural DNA[43b,c], our result suggests that, similar to natural DNA, hole transfer (motion of an oxidative charge) through xDNA in solution is likely to occur preferentially by hopping between x-guanine sites, as far as the xA−T intervening bridges are short.[43] However, electron-transfer coupling matrix elements are mandatory toward a quantitative estimation of the process efficiency and for a more rigorous description. In addition, this speculation should be tested against experimental data, which are currently totally missing.

Another electronic structure characteristic of x-bases is that the HOMO and LUMO Kohn−Sham orbitals for all of them have π character (see insets of Figure 2), with contribution of π electrons of the benzene ring.[17] In the natural DNA bases, instead, while the LUMOs are π orbitals for all of the bases, the HOMOs have a σ character for the pyrimidines (see, e.g., insets of Figures 2 and 3 in ref 39).

Turning to the inspection of the excited-state properties, we show in Figure 2 the calculated dipolar strength functions of the isolated x-bases, together with the Kohn−Sham HOMO and LUMO isosurface plots. The dipolar strength function is calculated by eq 1, that is, averaging the dynamical polarizabilities along the three spatial directions. Although we do not present a polarization-resolved analysis, we mention here that, by plotting separately the curves for the different light polarizations, one sees, as expected, that the absorption spectrum is highly anisotropic. This is due to the fact that at low energy, the bright excited states, namely, the absorption peaks with a detectable intensity, are prevalently of $\pi\pi^*$ character. Such excitations are not allowed by excitation of light polarized perpendicular to the base plane, and consequently, the dipolar strength function in the low-energy part of the spectrum for perpendicular polarization is 1 order of magnitude smaller than for that for in-plane polarizations.

In Figure 3, we report for comparison the absorption spectra measured for xDNA nucleosides in methanol, adapted from refs 9 and 11. We are aware that the systems simulated by us do not correspond exactly to the experimental conditions. However, we attempt a qualitative benchmark toward the only available experimental data. The experiment−theory environment differences consist essentially of (i) our simulations being in the gas phase, whereas the experiments were done with a methanol solution and (ii) our neglect of the backbone for computational efficiency.[39] Note that the effect of a solvent may be crucial for an exact matching of the computational results with experimental data.[24a,44,45] The neglect of the sugar−phosphate backbone, on the contrary, should not be relevant in the energy range in which we are interested (3−6 eV), as the sugar and the phosphate contributions to the absorption spectra only start to be important at higher energies. For instance, no backbone-induced signal was detected below ∼6 eV in the optical conductivity of different DNA sequences computed by DFT.[46]

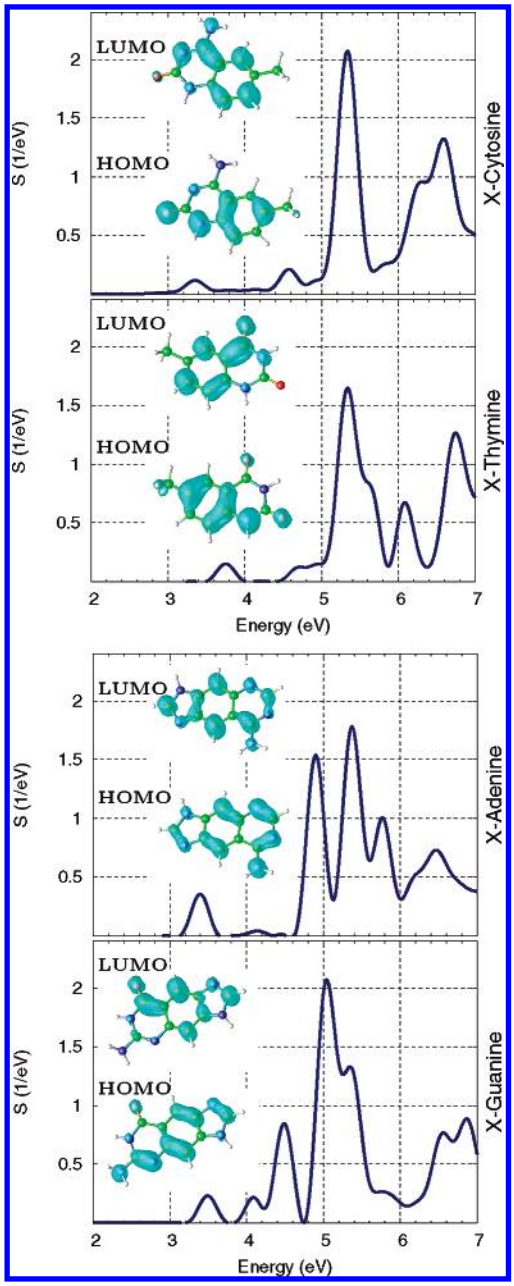

Figure 2. Calculated dipole strength functions of isolated gas-phase x-bases, averaged along the three real-space axes. Insets: isosurface plots of the HOMO and LUMO Kohn−Sham squared wave functions. Atoms of different chemical elements are indicated with spheres of different colors: carbon (green), nitrogen (blue), oxygen (red), and hydrogen (white).

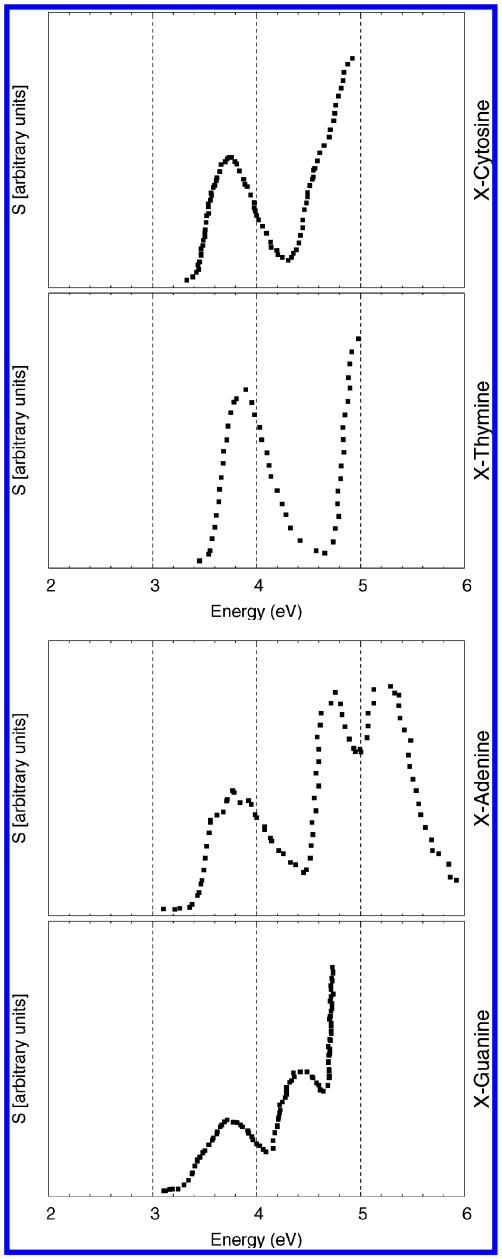

Figure 3. Experimental absorption spectra of size-expanded xDNA nucleosides in methanol. (Adapted from ref 9 for dxA and dxT and from ref 11 for dxG and dxC.)

TABLE 2: Vertical Excitation Energies (eV) Calculated for the Size-Expanded xDNA Bases

x-cytosine	x-thymine	x-adenine	x-guanine
3.35	3.75	3.40	3.49
4.16	4.71	4.15	4.09
4.57	5.33	4.45	4.49
5.33	5.62	4.90	5.04
		5.37	5.35

The experimental spectra of Figure 3 can be commented on by pointing out a couple of features for all of the size-expanded nucleobases. The first one is the presence of an absorption peak at low energy below 4 eV, in contrast to the natural DNA bases for which the absorption onset is always above 4.4 eV.[39] This peak is therefore induced by the presence of the benzene ring and is an optical fingerprint of the aromatic expansion. The second feature is the rise of the signal at higher energies and the presence of more intense peaks.

The results of our calculations, collected in Table 2, are in qualitative agreement with the experiments in revealing such features. In fact, Figure 2 shows that the low-energy peak, below 4 eV, is present in the theoretical spectra of all of the x-bases. A quantitative comparison, however, shows an underestimation of the energy of this peak, by less than 0.2 eV for xT, xA, and xG and by 0.39 eV for xC. Regarding higher-energy peaks, we detect more intense peaks in the range of ∼5−6 eV. A direct comparison with experiment is not possible because of the restricted measured energy range so that the experimental spectra are interrupted before 5 eV. Only for xA does the measured spectrum cover a larger energy range, and we can attempt a closer experiment−theory matching and interpretation. In the experimental absorption spectrum of xA (Figure 3), we can see the presence of two peaks at 4.76 and 5.36 eV, with quite the same dipole strength. Our calculations for xA reproduce such

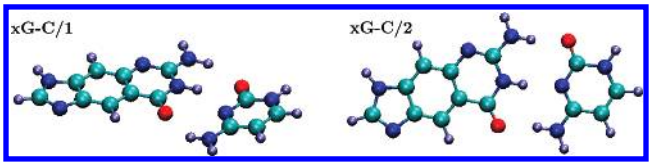

Figure 4. Two different investigated structures of the H-bonded xG−C pair. The x-pair xG−C/1 (left) is extracted from NMR measurements and is characterized by significant deviations from planarity. The x−pair xG-C/2 is instead planar and was constructed using standard distances for the Watson−Crick pattern.

a double-peak part of the curve; we find two peaks at 4.90 and 5.37 eV, in very good agreement with the measurement. In the case of xG, a clear absorption peak is measured at 4.41 eV, followed by a further intensity increase. This behavior of xG is also well reproduced by our calculation. In fact, we find a peak at 4.49 eV with an intensity intermediate between the onset peak and the most intense peaks that develop at higher energies. The calculated energies of the spectral maxima are collected in Table 2. In summary, the results of our time-dependent calculations of the excitation spectra of xDNA bases in the gas phase show a qualitative agreement with the experimental data in representing the overall shape of the absorption spectra and a fair quantitative agreement in the energies of the peaks.

IV. H-bonded x-Bases

As in natural DNA, hydrogen bonding is the lowest degree of aggregation toward more complex supramolecular architectures; also in xDNA, hydrogen bonding is the basic paradigm of interbase aggregation. An xDNA duplex[8,10] is composed of stacked x-pairs, and each x-pair is made of a benzo-fused base and a natural complementary base, that is, benzopurines are paired with pyrimidines and benzopyrimidines with purines.[8,10] Here, we present the computed optical properties of three H-bonded x-pairs each formed by a benzopurine and a pyrimidine, namely, xG−C and xA−T. As in the case of isolated bases, we have neglected the backbone.The xG−C pair was studied in two different conformations. One conformation was derived from an octamer xDNA double helix with the sequence d(xT−G−xT−A−xC−xG−C−xA−xG−T), whose structure was resolved by NMR.[15]The desired xG−C pair was extracted from the middle of the first best representative conformer of this segment contained in the 2ICZ pdb file, namely, the residues indicated as 7:14 in ref 15. The conformation obtained after omitting the backbone atoms from the pdb file is shown in Figure 4 (left), and from now on, we refer to it as xG−C/1. Another conformation was built on purpose. To avoid the uncertainty in the relative base orientation characteristic of the NMR xDNA fragment and the evident strong distortions probably due to the short oligomer length, we have also considered an ideal planar structure. This was constructed by pairing the planar xG base with a planar cytosine. For this assembly, we assumed the standard structural parameters that are valid for the hydrogen bonding between guanine and cytosine in natural DNA.[47] We expect that the insertion of benzene into the natural nucleobase does not significantly affect the hydrogen-bonding disposition of natural nucleobases.[8,20,21] The ideal conformation of xG−C is also shown in Figure 4 (right), and we refer to it as xG−C/2. The two target conformations (Figure 4) of the xG−C pair differ essentially in the planarity. This structural difference does not result in an appreciable difference in the fundamental ground-state electronic properties at the LDA level. The HOMO−LUMO gap is 2.14 and 2.05 eV for xG−C/1 and xG−C/2, respectively. In both cases we find that the HOMO (LUMO) charge distribution is

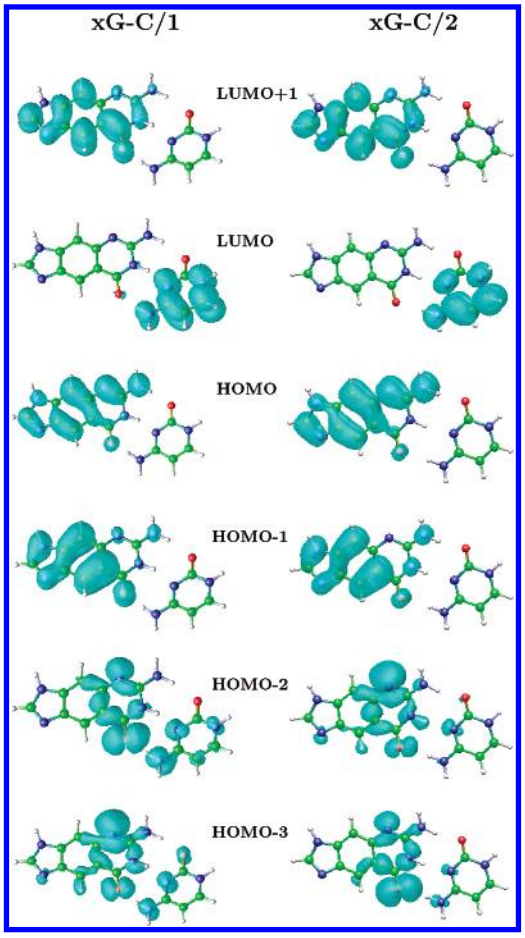

Figure 5. Isosurfaces of a few Kohn−Sham orbitals around the HOMO−LUMO gap for xG−C/1 (left) and xG−C/2 (right). These are the most important states involved in the low-energy part of the spectra of Figure 6, although the contribution of other occupied and unoccupied states is not fully negligible.

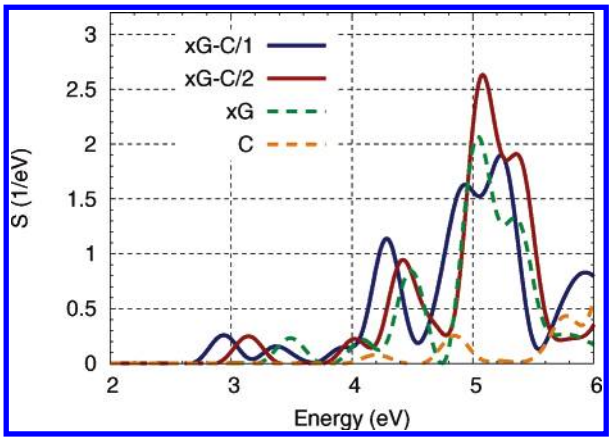

Figure 6. Calculated dipole strength function of gas-phase xG−C pairs in conformations 1 (solid blue) and 2 (solid red) (see Figure 4), averaged along the three real-space axes. The calculated dipole strength function of isolated xG (dashed green) and C[39] (dashed yellow) are also shown for comparison. The polarization-resolved signal for xG−C/1 is reported in the Supporting Information.

localized entirely in the xG (C) moiety (see Figure 5). The LUMO wave function is very similar to that of an isolated cytosine.[39]

The calculated dipole strength functions of the xG−C/1 and xG−C/2 pairs, averaged along the three real-space axes, are shown in Figure 6. In the same figure, we plot also the dipole strength functions of the isolated xG and C bases to reveal the

TABLE 3: Vertical Excitation Energies (eV) Calculated for the xDNA Hydrogen-Bonded Pairs

xG−C/1	xG−C/2	xA−T
2.94	3.14	3.12
3.37		3.55
3.94	4.03	4.23
4.29	4.43	4.71
4.93	5.08	5.26
5.23	5.36	5.72

effects induced by H bonding. The absorption spectrum of cytosine reported in Figure 6 was previously computed[39] with methodological details compatible with those of the present calculations. The calculated energies of the spectral maxima for the two conformations of xG−C are listed in Table 3. Looking at Figure 6, we first observe that the expanded nucleobase (xG) excitations have overall larger oscillator strengths than those of the natural base (C). For this reason, in both conformations, the spectra of the pairs are very similar in shape to the spectrum of isolated xG, and the excitations coming from the C moiety are somehow hidden by the more intense signal of xG. Comparing the spectra of the xG−C pairs with respect to the xG and C spectra, the main effect of the H bonding is a red shift of the low-lying excitations. This effect, known as a fingerprint of hydrogen bonding in the optical absorption spectra of natural DNA,[39,48,49] is thus preserved upon the chemical modification that produces xDNA. In xDNA, the low-frequency red shift is even enhanced.

The first excitation of xG−C has a $\pi\pi^*$ nature. As noted in the previous section, the natural bases have an absorption onset peak at higher energies than that of the benzo-fused bases; in particular, cytosine does not contribute to the optical absorption at energies lower than 4 eV (dashed yellow curve in Figure 6). Consequently, the lowest-energy excitation of xG−C (both xG−C/1 and xG−C/2) is clearly a local excitation that involves π electrons of the xG base and can be compared with the excitation energy of the lowest $\pi\pi^*$ singlet state of xG calculated at the same level of theory (green dashed line). It can be seen that for xG, complexation with cytosine stabilizes the lowest $\pi\pi^*$ singlet state by 0.55 eV in the case of xG−C/1 and by 0.35 eV in the case xG−C/2. A simple explication of this red shift can be given at the single-particle level by looking at the Kohn−Sham energy difference between the xG-localized electronic levels that define the first possible $\pi\pi^*$ transition, namely, the HOMO and the LUMO+1 (see Figure 5). These orbitals are the most important states involved in the main collective excitation, although the contribution of several other occupied and unoccupied states is not negligible. The single-particle energy difference between the HOMO and the LUMO+1 is 2.51 and 2.76 eV for xG−C/1 and xG−C/2, respectively, which means that it is by 0.53 (xG−C/1) and 0.28 eV (xG−C/2) smaller than the HOMO−LUMO gap of xG. Note that the HOMO (LUMO+1) of xG−C is identical to the HOMO (LUMO) of xG. These shifts essentially account for the energy red shifts found in the TDDFT excitation energies.

The red shift is larger for the xG−C/1 pair than that for the xG−C/2 pair. In addition, the former system is characterized by the appearance of an extra low-frequency peak at 3.37 eV, absent in xG−C/2. The origin of this extra peak can be understood again by inspecting the Kohn−Sham single-electron orbitals of Figure 5. We see that in the xG−C/1 pair, the HOMO−3 and HOMO−2 wave functions have a part of π-like distribution on cytosine. This is at odds with the situation for the xG−C/2 pair, whose HOMO−3 and HOMO−2 have just a tiny distribution on cytosine, of σ-like character. Thus, while

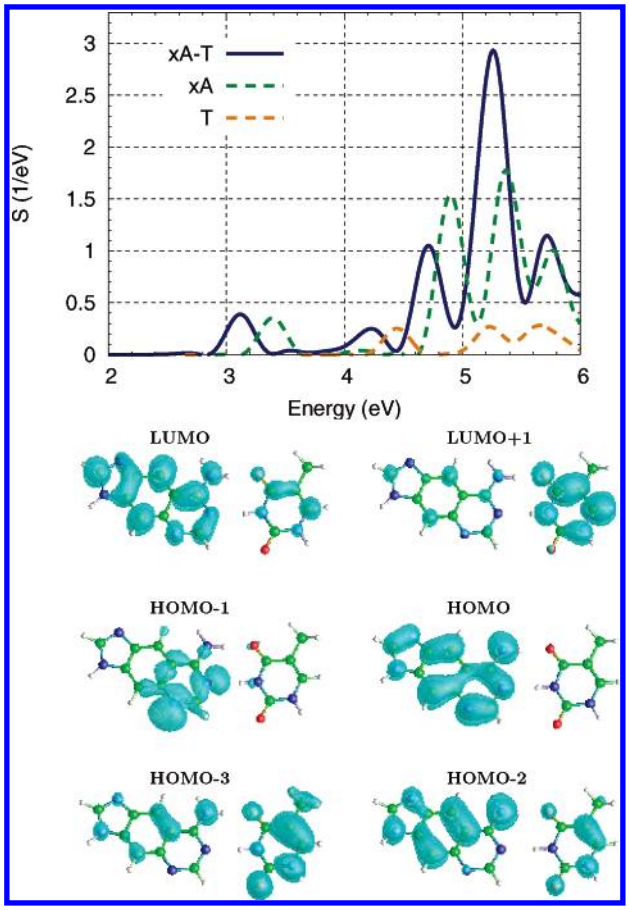

Figure 7. Top: Calculated dipole strength function of the gas-phase xA−T pair (solid blue), averaged along the three real-space axes. The calculated dipole strength functions of isolated xA (dashed green) and T (dashed yellow) are also shown for comparison. Bottom: Isosurfaces of Kohn−Sham orbitals of the xA−T pair around the HOMO−LUMO gap.

$|\text{HOMO}-2\rangle \rightarrow |\text{LUMO}\rangle$ and $|\text{HOMO}-3\rangle \rightarrow |\text{LUMO}\rangle$ transitions are symmetry forbidden in xG−C/2, they become allowed in xG−C/1, and they are most likely responsible for the extra peak at 3.37 eV. The Kohn−Sham energy differences of these two transitions are, in fact, 3.26 and 3.39 eV, respectively, quite similar to the TDDFT excitation energies. This kind of excitations implies a charge transfer between xG and C and can be likely ascribed to a charge-transfer state. Charge-transfer states are usually dark or have a very low oscillator strength for light-induced electronic excitations. We warn the reader that the identification of charge-transfer transitions is to be taken with care at the current level of TDDFT when a local or gradient-corrected exchange−correlation functional is used.[50−52]

Next, we turn the discussion to the other x-pair, composed of a benzo-fused adenine and a thymine (xA−T). The structure of this x-pair was extracted by a segment of duplex xDNA composed of 10 xA−T pairs. This xDNA was synthesized and analyzed with NMR,[13] and we obtained the NMR coordinates from the authors. From the pdb file for the whole duplex, we have extracted a base pair located in the middle of the oligomer, namely, the residues 5:16 of Figure 1 in ref 13, and we have omitted the backbone atoms. The calculated Kohn−Sham HOMO−LUMO gap at the LDA level for this structure is 2.52 eV. The HOMO and LUMO isosurface plots are presented in the bottom part of Figure 7 together with the first occupied and unoccupied states. We observe from these plots that while the HOMO wave function is completely localized on the xA base and has a complete π character, the LUMO has also a π

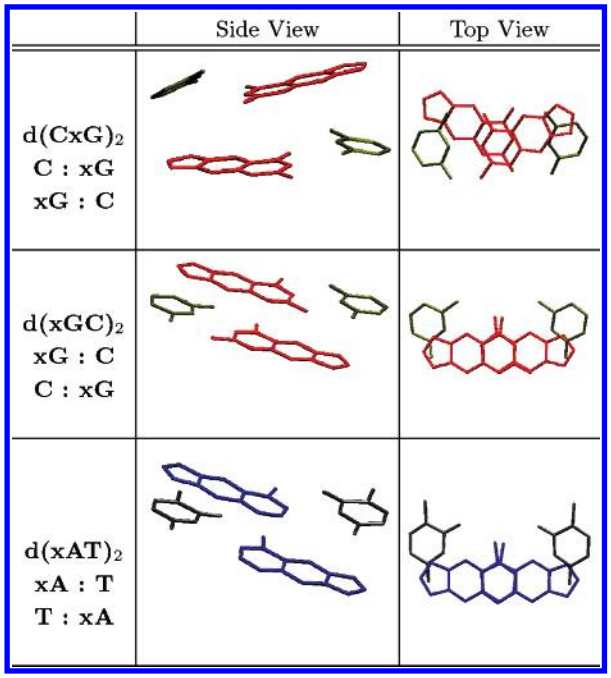

Figure 8. Atomic structures of the investigated stacks, in a ball and stick representation. Top: $d(CxG)_2$ irregular conformation extracted from the NMR measurement of an xDNA segment that contains all of the benzo-fused bases and possible H-bonded x-pairs.[15] Middle: $d(xGC)_2$ regular conformation constructed from the NMR average parameters valid for an xDNA segment that contains only xA−T pairs.[13] Bottom: $d(xAT)_2$ structure extracted from the NMR measurement of an xDNA segment containing only xA−T base pairs.[13] Different bases are indicated with different colors: xG(red), C(green), xA(blue), and T(black).

character, but a nonnegligible amount of charge is spread on the thymine molecule. This result is very similar to the B3LYP results of Fuentes-Cabrera and co-workers,[22] who found the same feature on a nucleotide pair of xA−T taking into account the backbone and using a saturation scheme where a H atom is put 1.0 Å away from the oxygen O2P (See Figure 8 of ref 22).

The calculated dipole strength function of the xA−T pair, averaged along the three real-space axes, is shown in Figure 7. As done for the analysis of the xG−C pairs, we also plot in Figure 7 the dipole strength functions of the isolated bases xA and T (dashed lines) to reveal the effects induced by H bonding. The calculated energies of the spectral maxima are listed in Table 3. Similar to the case of the xG−C pairs (Figure 6), we see that the major effect of H bonding in the selected xA−T pair is a red shift of the low-energy excitation peaks with respect to the isolated monomer excitations. Moreover, we see a relevant change in the relative spectral weights of the two peaks that are found in the xA signal around 5 eV. The red shift of the lowest-energy peak is 0.26 eV, and as was previously observed in the case of the xG−C pairs, also here, this shift can be attributed to an overall reduction of the $\pi\pi^*$ gap of xA induced by H-bond complexation by 0.31 eV with respect to the case of isolated xA. The same shift was also obtained at the B3LYP level comparing the HOMO−LUMO gap found for xA−T in ref 22 and for xA alone in ref 17. The peak at 4.23 eV presents a downward shift by 0.21 eV with respect to the first excitation energy of thymine. Again, a rationale for this shift can be obtained from a close look at the single-particle orbitals and energy levels. In the bottom of Figure 7, we see that the topmost occupied π states of xA−T that possess a charge component on the thymine are mixed orbitals, having charge density in both xA and T, hence with no counterpart in the isolated bases. In isolated thymine, the lowest-energy peak is due to the $|\mathrm{HOMO}-1\rangle \rightarrow |\mathrm{LUMO}\rangle$ transition. The HOMO−1 of isolated thymine is transformed in the xA−T pair into the two mixed orbitals HOMO−2 and HOMO−3 represented in Figure 7, and we attribute the peak at 4.23 eV in the solid curve of Figure 7 to a combination of the resulting transitions $|\mathrm{HOMO}-2\rangle \rightarrow |\mathrm{LUMO}\rangle$ and $|\mathrm{HOMO}-3\rangle \rightarrow |\mathrm{LUMO}\rangle$. In fact, in xA−T, the Kohn−Sham energy difference between the HOMO−2 (HOMO−3) and the LUMO is 0.26 eV (0.20 eV) smaller than the energy difference between the HOMO−1 and the LUMO of thymine, thus explaining the red shift of the peak found in xA−T at 4.23 eV.

These interpretations that are based on the single-particle DFT energy spectra are only indicative because in TDDFT, the difference of one-particle eigenvalues is renormalized by the Coulomb and exchange−correlation terms, including contributions from virtual particle−hole excitations that involve several occupied and unoccupied states. Therefore, a peak revealed in the absorption spectrum is usually determined by multiple transitions. However, any peak is usually dominated by one particular transition, and from a qualitative point of view, the assignments discussed above allow one to gain insights in a reliable way.

V. Stacked x-Bases

In the previous section, our aim was to understand what happens in the optical absorption spectra of xDNA bases when a benzopurine and a pyrimidine dimerize through hydrogen bonding. Here, we investigate the impact on the optical absorption spectra of the other kind of interaction typical of nucleic acids, namely, the stacking interaction. It has been speculated that the enhanced thermodynamic stability of xDNA with respect to B-DNA is a result of increased stacking due to the larger aromatic surface of the x-bases.[13] The stacking interaction is also increased for geometrical reasons because a conspicuous overlap between x-purines is found when they are placed in opposing strands.[21]

We considered three different fragments of two stacked x-pairs in which each x-pair is formed by a benzopurine and a pyrimidine, two stacks of xG−C pairs and one stack of xA−T pairs with the benzopurines on opposite strands, as illustrated in Figure 8. The stacked geometries are indicated in the following with a subscript that stands for the number of H-bonded pairs that form the stack.

The first $(xG-C)_2$ stack, labeled with $d(CxG)_2$ and shown in the top part of Figure 8, is taken again from the NMR study of an xDNA duplex containing all of the eight possible x-pairs formed by a benzo-fused base and a natural base;[15] from the pdb file, we have extracted the residues indicated as 7:14 and 6:15 in ref 15 and omitted the backbone atoms. This $d(CxG)_2$ structure derived from the real fragment is rather asymmetric. In order to avoid spurious conclusions dictated by the pronounced asymmetries that may likely be smeared by averaging over several snapshots, we have also studied another idealized, more regular structure characterized by enhanced overlap between xG bases in opposite strands. The second $(xG-C)_2$ stack, shown in the middle part of Figure 8 and named $d(xGC)_2$, has been constructed by applying the helical symmetry with the average structural parameters contained in Table 3 of ref 13, starting from the planar H-bonded xG−C pair of section IV.[53]

The simulated $(xA-T)_2$ stack, labeled $d(xAT)_2$ and shown in the bottom panel of Figure 8, was taken from the NMR structure of an xDNA duplex containing only xA−T H-bonded

pairs.[13] From the pdb file, we extracted the residues indicated as 5:16 and 6:15 in Figure 1 of ref 13 and omitted the backbone atoms. In this case, the NMR coordinates exhibit the desired overlap between the x-bases (Figure 8).

The Kohn−Sham energy gap for the two $(xC-C)_2$ stacks are 2.07 eV for $d(CxG)_2$ and 2.12 eV for $d(xGC)_2$, very similar to the H-bonded x-pairs xG−C/1 and xG−C/2. The two highest occupied molecular orbitals have a charge density distribution localized on the xG's in opposite strands, and they are split in energy due to the stacking interaction. In the case of the regular $d(xGC)_2$ stack, two such orbitals are localized on both xG's, and their energy separation is 0.24 eV. In the case of the irregular $d(CxG)_2$ stack, one of such two orbitals is fully localized on the xG of the upper plane and the other one on the xG of the lower plane, and their energy separation is 0.19 eV. The two lowest unoccupied molecular orbitals are instead much more degenerate. In the case of the $d(xGC)_2$ stack, one is localized on the upper cytosine and the other on the lower cytosine, and the energy separation is 0.09 eV. In the case of the $d(CxG)_2$ stack, they are both localized on both cytosines, and the energy separation is 0.014 eV. Isosurface plots of the wave functions of electron states around the HOMO−LUMO gap are reported in the Supporting Information, as well as the energy level diagrams. In summary, for $(xG-C)_2$ stacks, the HOMO/HOMO−1 orbital duplet derives from the HOMO of the H-bonded xG−C pairs and maintains a benzopurine character as in the isolated pair. The same consideration applies to the LUMO/LUMO+1 orbital duplet, and this derives from the pyrimidine-localized LUMO of the isolated H-bonded pair and maintains the purely pyrimidine character.

For the $d(xAT)_2$ stack, we find instead more orbital mixing. The two highest occupied (lowest unoccupied) molecular orbitals do not maintain the purely benzopurine (pyrimidine) character that the parent HOMO and LUMO have in the isolated xA−T H-bonded pair (Supporting Information). The HOMO maintains a π character on benzoadenine, but the HOMO−1 is partly spread on thymine. In the unoccupied part of the spectrum, we find instead a quadruplet of levels with wave functions spread on both xA and T. This can be understood by comparing with the energy levels of the isolated xA−T pair; in fact, while in xG−C the LUMO is well separated in energy from the LUMO+1, in xA-T, the LUMO and LUMO+1 have a small energy separation (Supporting Information), and therefore, they mix easily upon stacking and give origin to the LUMO-derived quadruplet instead of a LUMO-derived duplet. The Kohn−Sham energy gap for this structure is 2.08 eV, reduced by 0.44 eV with respect the xA−T H-bonded pair. Note that such an enhanced mixing among the purine and pyrimidine orbitals does not occur in natural A−T pairs and in xA−T pairs finds its origin in the shifts of energy levels in the electronic structure of x-bases.[17]

The calculated dipole strength functions are plotted in Figure 9 for $d(xGC)_2$ and $d(CxG)_2$ and in Figure 10 for $d(xAT)_2$. In each panel, we also plot the linear combination of the absorption spectra of two independent H-bonded x-pairs. In the top (bottom) panel of Figure 9, the dipole strength function of the $d(CxG)_2$ ($d(xGC)_2$) stack is compared to the double signal of the parent xG−C pair, that is, xG−C/1 (xG−C/2).[54] We observe that, overall, the absorption peaks occur at the same energies as the peaks of the component H-bonded x-pairs. Differences are found in the relative strengths of some peaks; in $d(xGC)_2$, the intensity ratio between the excitations at 4.03 and 4.43 eV is inverted with respect to the case of the xG−C/2 pair. In $d(CxG)_2$, we reveal a small total downward shift and a huge depression of

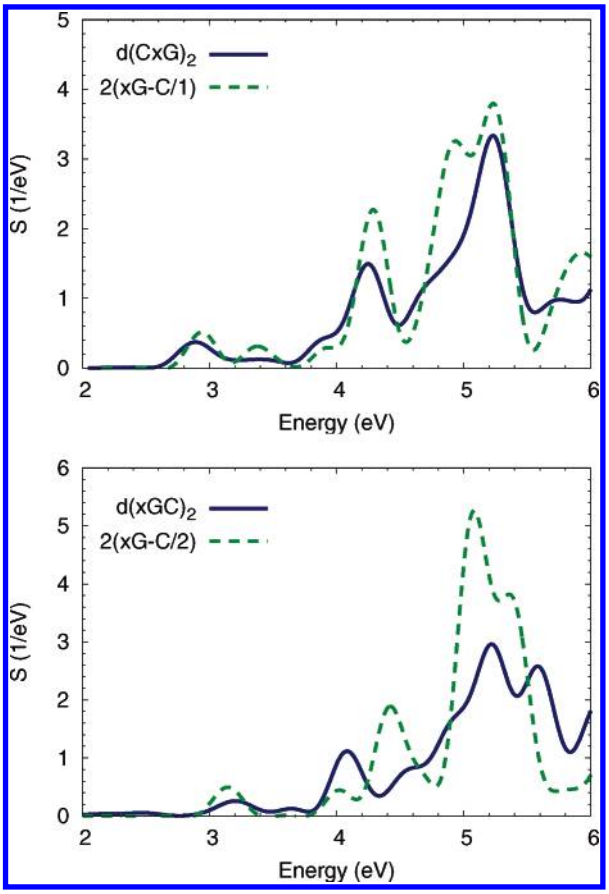

Figure 9. Top: Calculated dipole strength function of the gas-phase $d(CxG)_2$ stack averaged along the three real-space axes (solid blue). Bottom: Calculated dipole strength function of the gas-phase ideal $d(xGC)_2$ stack. In each panel, the double of the xG−C/1 (up) and xG−C/2 (down) spectrum is also shown with the green dotted line.

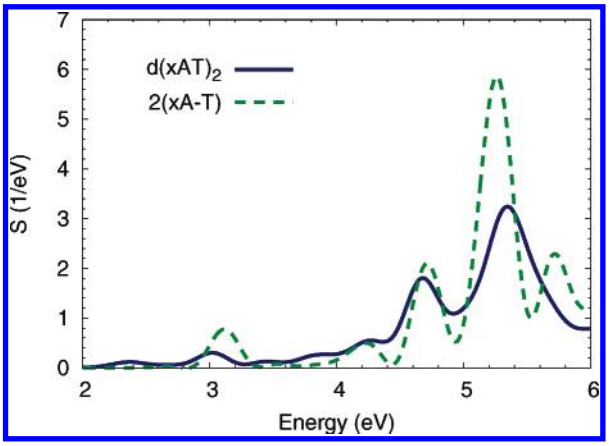

Figure 10. Top: Calculated dipole strength function of the gas-phase $d(xAT)_2$ stack averaged along the three real-space axes (solid blue). The double of the xA−T pair spectrum is also shown with the green dotted line.

the peak at 4.93 eV, while the peak at 5.23 eV maintains an intensity comparable to that of the isolated xG−C/1 pair. Also for $d(xAT)_2$, the shape of the spectrum appears to be very similar to that of a single xA−T pair, as emerges from Figure 10.

The common feature of all of the studied stacked structures is an evident quenching of the intensity of all of the peaks. This decrease is a typical effect of the stacking arrangement, as was already pointed out by us and other authors for natural DNA[39] and other forms.[55] Comparing the peak intensities to the intensities that the corresponding peaks have in the signal

obtained as the linear combination of the parent H-bonded x-pairs, we find for $d(CxG)_2$ and $d(xGC)_2$, respectively, a reduction by 27 and 43% for the first peak and 12 and 44% for the most intense peak. For $d(xAT)_2$, the reduction is 64% for the first peak and 44% for the most intense peak. Summarizing this section, we have shown that the stacks do not present major discrepancies with respect to the parent H-bonded x-pairs. Slight differences appear in both the low-energy and high-energy ranges but without significant shifts that would be the index of remarkable changes in the transitions that contribute to the peaks. While H bonding is responsible for the major shifts with respect the isolated bases, the main effect of the stacking arrangement is the pronounced hypochromicity.[56] These features are very similar to natural DNA. It is well-known that the hypochromicity effect is very important because the intensity change may be exploited to follow the melting of the secondary structure of nucleic acids[55,57,58] when varying the temperature or environmental parameters and reveals distinctive features of various DNA forms. In the case of xDNA, the results of our calculations indicate that hypochromicity is stronger for the two structures with a regular overlap between x-pairs with the x-purines in opposite strands, namely, $d(xGC)_2$ and $d(xAT)_2$ rather than $d(CxG)_2$ (see left panel of Figure 8). We note that Mergny and co-workers recently pointed out the efficacy of thermal difference spectra to characterize the folding and unfolding of nucleic acids, also observing that while the main peak is usually effected by hypochromicity upon folding, hyperchromicity may be revealed at some frequencies where $n-\pi^*$ transitions are relevant.[55] These experimental studies, and our limited theoretical findings for natural DNA and xDNA, open the way to more extensive theoretical investigation of the hypochromicity and hyperchromicity in nucleic acids, for instance, by simulating optical absorption spectra of intermediate configurations that occur during the unfolding of DNA. In principle, one could conduct classical molecular dynamics simulations to identify low-energy intermediates and then carry out quantum mechanical calculations of the optical properties of few selected intermediates. Such calculations at the ab initio level are still very demanding and way beyond the scope of this study.

VI. Conclusion

In this article, we have presented the results of TDDFT calculations of the optical absorption spectra of xDNA bases and some representative base complexes that exhibit the main interactions typical of nucleic acids, namely, H bonding and stacking.

For the isolated benzo-fused bases xA, xG, xT, and xC, we find a fairly good qualitative agreement with measured data in the energy range where experimental results are available. Our benchmark to assess the agreement is the appearance of the peak of absorption onset at an energy smaller than that proper of any natural nucleobase; this onset peak is the novel feature induced by the benzene−base fusion. We find its intensity in all of the x-bases depressed with respect to the experimental signal, but its energy is much better estimated, and indeed, its very presence is in strong support of our methodology.

For the H-bonded x-pairs that we have included in our study, we find conspicuous red shifts, especially for the low-energy peaks. This feature is in common with natural DNA, although the entity of the shifts varies from system to system. In addition to the red shifts that are common for all of the simulated H-bonded x-pairs, we find the appearance of a new low-energy peak in the nonplanar structure xG−C/1, dominated by transitions that are not allowed for the more regular planar systems and due to mixing between benzopurine and pyrimidine orbitals.

For the stacked complexes, the main trait is the pronounced hypochromicity, which is largest for the planar structures where the stacking interactions are mostly favored. Hypochromicity is another feature that is in common with natural DNA, and we find it more pronounced in the model xDNA stacks because of the enhanced interplane overlap. The next compelling issue is whether or not the enhanced stacking has consequences on the conductance and rates of electron/hole transfer; studies are ongoing in our group and will be addressed in forthcoming reports.

Acknowledgment. We are grateful to Agostino Migliore, Stefano Corni, Arrigo Calzolari, and Angel Rubio for fruitful discussions. We thank Eric Kool for providing us with the coordinates of the xDNA oligomer investigated in ref 13. This work was supported by the European Commission through Contracts N. FP6-029192 (IST FET-Open project "DNA-NANODEVICES") and N. NMP4-CT-2004- 500198 (NMP NoE "NANOQUANTA") and by INFM-CNR through the Parallel Computing Committee.

Supporting Information Available: Figures S1 and S2 show the LDA energy levels of the structures xG−C/1, xG−C/2, $d(CxG)_2$, $d(xGC)_2$, xA−T, and $d(xAT)_2$; Figure S3 shows the polarization-resolved dipole strength functions of the xG−C/1 structure; Table S1 collects isosurface plots of relevant orbitals around the HOMO−LUMO gap for the structures $d(CxG)_2$, $d(xGC)_2$, and $d(xAT)_2$. This material is available free of charge via the Internet at http://pubs.acs.org.

References and Notes

(1) Henry, A. A.; Romesberg, F. E. *Curr. Opin. Chem. Biol.* **2003**, *7*, 727.

(2) Di Felice, R.; Porath, D. In *NanoBioTechnology: BioInspired Devices and Materials of the Future*; Shoseyov, O., Levy. I., Eds.; Humana Press: Totowa, NJ, 2007; ISBN13: 978-1-58829-894-2, ISBN10: 1-58829-894-9.

(3) Kool, E. T.; Waters, M. L. *Nat. Chem. Biol.* **2007**, *3*, 70.

(4) Benner, S. A. *Nature* **2003**, *421*, 118.

(5) Krueger, A. T.; Lu, H.; Lee, A. H.; Kool, E. T. *Acc. Chem. Res.* **2007**, *40*, 141.

(6) Hirao, I. *Curr. Opin. Chem. Biol.* **2006**, *10*, 622.

(7) Kool, E. T. *Acc. Chem. Res.* **2002**, *35*, 936.

(8) Liu, H.; Gao, J.; Lynch, S. R.; Saito, Y. D.; Maynard, L.; Kool, E. T. *Science* **2003**, *302*, 868.

(9) Liu, H.; Gao, J.; Maynard, L.; Saito, Y. D.; Kool, E. T. *J. Am. Chem. Soc.* **2004**, *126*, 1102.

(10) Gao, J.; Liu, H.; Kool, E. T. *Angew. Chem., Int. Ed.* **2005**, *44*, 3118.

(11) Liu, H.; Gao, J.; Kool, E. T. *J. Org. Chem.* **2005**, *70*, 639.

(12) Gao, J.; Liu, H.; Kool, E. T. *J. Am. Chem. Soc.* **2004**, *126*, 11826.

(13) Liu, H.; Lynch, S. R.; Kool, E. T. *J. Am. Chem. Soc.* **2004**, *126*, 6900.

(14) Liu, H.; Gao, J.; Kool, E. T. *J. Am. Chem. Soc.* **2005**, *127*, 1396.

(15) Lynch, S. R.; Liu, H.; Gao, J.; Kool, E. T. *J. Am. Chem. Soc.* **2006**, *128*, 14704.

(16) Di Felice, R.; Calzolari, A.; Garbesi, A.; Alexandre, S. S.; Soler, J. M. *J. Phys. Chem. B* **2005**, *109*, 22301.

(17) Fuentes-Cabrera, M.; Sumpter, B. G.; Wells, J. C. *J. Phys. Chem. B* **2005**, *109*, 21135.

(18) Fuentes-Cabrera, M.; Sumpter, B. G.; Lipkowski, P.; Wells, J. C. *J. Phys. Chem. B* **2006**, *110*, 6379.

(19) Fuentes-Cabrera, M.; Lipkowski, P.; Huertas, O.; Sumpter, B. G.; Orozco, M.; Luque, F. J.; Wells, J. C.; Leszczynski, J. *Int. J. Quantum Chem.* **2006**, *106*, 2339.

(20) Huertas, O.; Poater, J.; Fuentes-Cabrera, M.; Orozco, M.; Sola, M.; Luque, F. J. *J. Phys. Chem. A* **2006**, *110*, 12249.

(21) McConnell, T. L.; Wetmore, S. D. *J. Phys. Chem. B* **2007**, *111*, 2999.

(22) Fuentes-Cabrera, M.; Zhao, X.; Kent, P. R. C.; Sumpter, B. G. *J. Phys. Chem. B* **2007**, *111*, 9057.

(23) Omerzu, A.; Licer, M.; Mertelj, T.; Kabanov, V. V.; Mihailovic, D. *Phys. Rev. Lett.* **2004**, *93*, 218101.

(24) (a) Crespo-Hernández, C. E.; Cohen, B.; Hare, P. M.; Kohler, B. *Chem. Rev.* **2004**, *104*, 1977. (b) Crespo-Hernández, C. E.; Cohen, B.; Kohler, B. *Nature* **2005**, *436*, 1141.

(25) (a) Marguet, S.; Markovitsi, D. *J. Am. Chem. Soc.* **2005**, *127*, 5780. (b) Markovitsi, D.; Onidas, D.; Gustavsson, T.; Talbot, F.; Lazzarotto, E. *J. Am. Chem. Soc.* **2005**, *127*, 17130. (c) Gustavsson, T.; Sarkar, N.; Lazzarotto, E.; Markovitsi, D.; Barone, V.; Improta, R. *J. Phys. Chem. B* **2006**, *110*, 12843. (d) Markovitsi, D.; Talbot, F.; Gustavsson, T.; Onidas, D.; Lazzarotto, E.; Marguet, S. *Nature* **2006**, *441*, E7.

(26) Runge, E.; Gross, E. K. U. *Phys. Rev. Lett.* **1984**, *52*, 997.

(27) *Time-Dependent Density Functional Theory*; Marques, M. A. L., Ullrich, C., Nogueira, F., Rubio, A., Burke, K., Gross, E. K. U., Eds.; Springer: Berlin, Germany, 2006.

(28) Marques, M. A. L.; Castro, A.; Bertsch, G. F.; Rubio, A. *Comput. Phys. Commun.* **2003**, *151*, 60.

(29) Castro, A.; Appel, H.; Oliveira, M.; Rozzi, C. A.; Andrade, X.; Lorenzen, F.; Marques, M. A. L.; Gross, E. K. U.; Rubio, A. *Phys. Status Solidi B* **2006**, *243*, 2465. The code OCTOPUS is available at http://www.tddft.org/programs/octopus/

(30) Troullier, N.; Martins, J. L. *Phys. Rev. B* **1991**, *43*, 1993.

(31) Perdew, J. P.; Zunger, A. *Phys. Rev. B* **1981**, *23*, 5048.

(32) Casida E. In *Recent Advances in Density Functional Methods Part I*; Chong, D. P., Ed.; World Scientific: Singapore, 1995; p 115.

(33) Castro, A.; Marques, M. A. L.; Alonso, J. A.; Rubio, A. *J. Comput. Theor. Nanosci.* **2004**, *1*, 231.

(34) Marques, M. A. L.; Castro, A.; Rubio, A. *J. Chem. Phys.* **2001**, *115*, 3006.

(35) Yabana, K.; Bertsch, G. F. *Int. J. Quantum Chem.* **1999**, *75*, 55.

(36) Malloci, G.; Mulas, G.; Joblin, C. *Astron. Astrophys.* **2004**, *426*, 105.

(37) Marques, M. A. L.; Lopez, X.; Varsano, D.; Castro, A.; Rubio, A. *Phys. Rev. Lett.* **2003**, *90*, 258101.

(38) Lopez, X.; Marques, M. A. L.; Castro, A.; Rubio, A. *J. Am. Chem. Soc.* **2005**, *127*, 12329.

(39) Varsano, D.; Di Felice, R.; Marques, M. A. L.; Rubio, A. *J. Phys. Chem. B* **2006**, *110*, 7129.

(40) Castro, A.; Marques, M. A. L.; Alonso, J. A.; Bertsch, G. F.; Yabana, K.; Rubio, A. *J. Chem. Phys.* **2002**, *116*, 1930.

(41) Castro, A.; Marques, M. A. L.; Rubio, A. *J. Chem. Phys.* **2004**, *121*, 3425.

(42) Perdew, J. P.; Burke, K.; Ernzerhof, M.; *Phys. Rev. Lett.* **1996**, *77*, 3865.

(43) (a) Giese, B. In *Topics Curr. Chem.* **2004**, *236*, 27; Schuster, G., Ed. (b) Berlin, Y. A.; Kurnikov, I. V.; Beratan, D.; Ratner, M. A.; Burin, A. L. In *Topics Curr. Chem.* **2004**, *237*, 1; Schuster, G., Ed. (c) Rösch, N.; Voityuk, A. A. In *Topics Curr. Chem.* **2004**, *237*, 37; Schuster, G., Ed.

(44) Mennucci, B.; Tonniolo, A.; Tomasi, J. *J. Phys. Chem. A* **2001**, *105*, 4749.

(45) Mishra, S. K.; Shukla, M. K.; Mishra, P. C. *Spectrochim. Acta, Part A* **2000**, *56*, 1355.

(46) (a) Gervasio, F. L.; Carloni, P.; Parrinello, M. *Phys. Rev. Lett.* **2002**, *89*, 108102. (b) Hübsch, A.; Endres, R. G.; Cox, D. L.; Singh, R. R. P. *Phys. Rev. Lett.* **2005**, *94*, 178102.

(47) Arnott, S.; Hukins, D. W. L. *Biochem. Biophys. Res. Commun.* **1972**, *47*, 1504.

(48) Sobolewski, A.; Domcke, W. *Phys. Chem. Chem. Phys.* **2004**, *6*, 2763.

(49) Wesolowski, T. *J. Am. Chem. Soc.* **2004**, *126*, 11444.

(50) Dreuw, A.; Weisman, J. L.; Head-Gordon, M. *J. Chem. Phys.* **2003**, *119*, 2943.

(51) Dreuw, A.; Weisman, J. L.; Head-Gordon, M. *J. Am. Chem. Soc.* **2004**, *126*, 4007.

(52) Gritsenko, O.; Baerends, E. J. *J. Chem. Phys.* **2004**, *121*, 655.

(53) Note that the work by Kool and co-workers[13] from which we took the helical parameters to construct the $d(xGC)_2$ stack indeed reported the study of a fragment composed uniquely of xA−T pairs. Despite the fact that this experimental fragment does not contain xG−C pairs, we have taken from it the average structural parameters to build our idealized $(xG-C)_2$ stack because it is the only available sample containing only benzopurines and H-bonded x-pairs of a single type, which is expected to lead to a more regular conformation and optimized stacking.

(54) For the $d(CxG)_2$, this comparison is less rigorous than that for the two other stacked systems because the structure is not composed of two identical pairs. For full consistency, one should calculate the spectra for both the isolated H-bonded pairs forming the structure and sum them. However, our approximation is satisfactory for qualitative indications.

(55) Mergny, J.-L.; Li, J.; Lacroix, L.; Amrane, S.; Chaires, J. B. *Nucl. Acids Res.* **2005**, *33*, e138.

(56) Tinoco, I., Jr. *J. Am. Chem. Soc.* **1960**, *82*, 4785.

(57) Dolinnaya, N. G.; Fresco, J. R. *Proc. Natl. Acad. Sci. U.S.A.* **1992**, *89*, 9242.

(58) Cox, R. A. *Biochem. J.* **1970**, *120*, 539.